Geophysical Research Letters

RESEARCH LETTER
10.1029/2020GL089441

Key Points:
- There are few measurements of ultralow frequency (ULF) wave geoelectric fields (E_{GEO}), despite the hazard these fields can represent
- A coordinated investigation of ULF waves and E_{GEO} reveals significant spatial inhomogeneities in E_{GEO} related to Earth conductivity
- Measured storm time ULF wave E_{GEO} amplitudes of ~300–1000 mV/km suggest that they should be considered in future geoelectric hazard analysis

Supporting Information:
- Supporting Information S1
- Text S1
- Figure S1
- Figure S2
- Figure S3
- Movie S1

Correspondence to:
M. D. Hartinger,
mhartinger@spacescience.org

Citation:
Hartinger, M. D., Shi, X., Lucas, G. M., Murphy, B. S., Kelbert, A., Baker, J. B. H., et al. (2020). Simultaneous observations of geoelectric and geomagnetic fields produced by magnetospheric ULF waves. *Geophysical Research Letters*, *47*, e2020GL089441. https://doi.org/10.1029/2020GL089441

Received 21 JUN 2020
Accepted 29 AUG 2020

Simultaneous Observations of Geoelectric and Geomagnetic Fields Produced by Magnetospheric ULF Waves

M. D. Hartinger[1,2], X. Shi[2,3], G. M. Lucas[4], B. S. Murphy[5], A. Kelbert[5], J. B. H. Baker[2], E. J. Rigler[5], and P. A. Bedrosian[5]

[1]Space Science Institute, Boulder, CO, USA, [2]Department of Electrical and Computer Engineering, Virginia Polytechnic Institute and State University, Blacksburg, VA, USA, [3]High Altitude Observatory, National Center for Atmospheric Research, Boulder, CO, USA, [4]Laboratory for Atmospheric and Space Physics, University of Colorado Boulder, Boulder, CO, USA, [5]U. S. Geological Survey, Golden, CO, USA

Abstract Geomagnetic perturbations (B_{GEO}) related to magnetospheric ultralow frequency (ULF) waves induce electric fields within the conductive Earth—geoelectric fields (E_{GEO})—that in turn drive geomagnetically induced currents. Though numerous past studies have examined ULF wave B_{GEO} from a space weather perspective, few studies have linked ULF waves with E_{GEO}. Using recently available magnetotelluric impedance and E_{GEO} measurements in the contiguous United States, we explore the relationship between ULF waves and E_{GEO}. We use satellite, ground-based radar, B_{GEO}, and E_{GEO} measurements in a case study of a plasmaspheric virtual resonance (PVR), demonstrating that the PVR E_{GEO} has significant spatial variation in contrast to a relatively uniform B_{GEO}, consistent with spatially varying Earth conductivity. We further show ULF wave E_{GEO} measurements during two moderate storms of ~1 V/km. We use both results to highlight the need for more research characterizing ULF wave E_{GEO}.

Plain Language Summary A variety of phenomena in the near-Earth space environment produce disturbances in the magnetic field observed on the ground, including plasma waves in the ionized portion of the Earth's upper atmosphere. Though numerous studies have characterized magnetic disturbances related to waves with frequencies below a few hertz, few studies have addressed the electric fields they can induce in the Earth: geoelectric fields (E_{GEO}). The latter are important because they drive potentially damaging electrical currents in power grids and other infrastructure. This study addresses the lack of constraints on wave E_{GEO} fields by taking advantage of recently available models and measurements. The results show that extreme wave events can produce E_{GEO} of significant amplitude, comparable to once-per-century values obtained in other studies. The results also indicate that more work is needed to characterize wave E_{GEO}.

1. Relationship Between ULF Waves and Geoelectric Fields

Geomagnetic perturbations (B_{GEO}) related to a variety of phenomena in the near-Earth space environment induce electric fields at the Earth's surface. These geoelectric fields (E_{GEO}) in turn drive potentially damaging geomagnetically induced currents (GIC) in technological infrastructure such as power grids (e.g., North American Electric Reliability Corporation (NERC), 2012; Pulkkinen et al., 2017; Thomson, 2007). The GIC intensities depend on the spatial and temporal structure of geoelectric fields and the geometry and the electrical resistances of the technological infrastructure of interest; in other words, all GICs are fundamentally driven by geoelectric fields, although the particular relation between GICs and geoelectric fields depends upon the specific technological infrastructure. Thus, E_{GEO} is an important link between magnetospheric phenomena and GICs, and significant research effort is directed toward characterizing the geoelectric field (Kelbert et al., 2017; Love et al., 2019; Lucas et al., 2018, 2020), which can then be used to characterize GIC via tailored engineering assessments (Pulkkinen et al., 2017). As noted in section 3 of (Pulkkinen et al., 2017, page 833), " … the 'division of work' is now clear: science activities need to characterize the geoelectric field, which is the input for further engineering analyses."

Geoelectric fields can be measured directly (e.g., Ferguson, 2012) or estimated at a given position using

$$\mathbf{E_{GEO}}(\omega) = \frac{1}{\mu}\begin{pmatrix} Z_{xx}(\omega) & Z_{xy}(\omega) \\ Z_{yx}(\omega) & Z_{yy}(\omega) \end{pmatrix} \mathbf{B_{GEO}}(\omega) \quad (1)$$

where ω is the frequency, E_{GEO} and B_{GEO} are the frequency-dependent geoelectric and geomagnetic fields, **Z** is a tensor corresponding to an impedance from a magnetotelluric (MT) survey, and μ is the magnetic permeability (e.g., Bedrosian & Love, 2015). **Z** depends on the electrical conductivity of the Earth, which varies in three dimensions and is a function of rock composition, including physical, chemical, and thermal state. **Z** is an effectively stationary function (time independent for periods relevant to GIC) that can be used to map a time-varying B_{GEO} to E_{GEO}. Equation 1 also assumes a plane wave source, in which the inducing magnetic field at the Earth's surface is coherent over length scales larger than the skin depth of induced currents; this assumption holds for the B_{GEO} examined in this letter based on comparisons between measured and calculated geoelectric fields and the fact that the waves in this study have spatial scales of >∼1,000 km, significantly larger than the skin depth in the region of interest. Using Equation 1 with an assumed B_{GEO} and measured **Z**, Bedrosian and Love (2015) demonstrated that E_{GEO} can exhibit rapid spatial variations even in the presence of a spatially uniform B_{GEO}. In particular, they assumed monochromatic B_{GEO} with 1-, 10-, and 100-mHz frequency and spatially uniform amplitude; using **Z** (from MT survey) and Equation 1, they estimated E_{GEO} and found significant spatial variations related to variations in the electrical conductivity of the Earth.

The frequencies examined by Bedrosian and Love (2015) are in the ultralow frequency range (ULF) defined by Jacobs et al. (1964) to classify pulsations, or waves, in the magnetosphere-ionosphere system; in this work, we focus on waves with frequencies below 22 mHz, referred to as Pc5 (∼2–7 mHz), Pc4 (7–22 mHz, continuous wave train), and Pi2 (7–22 mHz, waves only last a few cycles) waves. Some types of ULF waves have spatially uniform amplitudes and polarizations very similar to the B_{GEO} assumed by Bedrosian and Love (2015). For example, the cold, dense plasma of the inner magnetosphere, or plasmasphere, can act as a resonator and partially trap ULF wave energy leading to a wave mode known as a plasmaspheric virtual resonance (PVR; Lee & Kim, 1999). PVR models predict a spatially uniform (amplitude and frequency) B_{GEO} at low and midlatitudes with roughly 100s period (Lee & Takahashi, 2006; Takahashi et al., 2009), appropriate for use with Equation 1. Shi et al. (2017) identified a PVR using ground magnetometer data from a similar geographic region as Bedrosian and Love (2015), finding waves very similar to the B_{GEO} imposed by Bedrosian and Love (2015): ∼1 nT spatially uniform amplitude (on scales ∼ >1,000 km) with 10-mHz frequency.

Several studies have demonstrated that magnetospheric ULF waves can drive intense GIC and thus represent a hazard (e.g., Belakhovsky et al., 2019; Pulkkinen & Kataoka, 2006). However, few studies have focused on ULF waves as a driver of E_{GEO}, despite the recognition by the GIC research community that geoelectric field constraints are needed for tailored engineering assessments and forecasting, in particular that "improved understanding and specification of the field over different spatial and temporal scales is needed" (Pulkkinen et al., 2017, pages 832–833). For example, ULF wave E_{GEO} are not generally covered in review papers and monographs examining a wide variety of ULF wave research (e.g., Keiling et al., 2016; McPherron, 2005; Takahashi et al., 2006), and there are few past reports of ULF wave E_{GEO} measurements. Motivated by these facts—and taking advantage of a recent, significant increase in the availability of B_{GEO}, E_{GEO}, and **Z** measurements in the contiguous United States—we have three objectives with this letter:

1. Section 2: Apply the Bedrosian and Love (2015) techniques, along with direct E_{GEO} measurements, to the event of Shi et al. (2017) to demonstrate how one particular ULF wave mode can drive E_{GEO}. This is the first coordinated investigation using satellite, ground-based radar, and spatially distributed B_{GEO}, E_{GEO}, and **Z** measurements to identify a specific magnetospheric ULF wave mode and link this wave mode to a spatial distribution of E_{GEO}.
2. Section 3: Use measured geoelectric fields during two additional storm time ULF wave case studies to characterize more extreme ULF wave E_{GEO}
3. Section 4: Place these results in context with past work to highlight the need for more research into the relationship between ULF waves and E_{GEO}.

2. Case Study: Geoelectric Fields Driven by a PVR

Shi et al. (2017) reported global Pi2 pulsations ("Pi2" refers to irregular, or lasting only a few wave cycles, pulsations with frequencies from 7–22 mHz) occurring on 25 September 2014, observed around a substorm onset at ~06:04 UT by space and ground-based instruments. Time History of Events and Macroscale Interactions during Substorms (THEMIS) satellites (Angelopoulos, 2008) measurements of in situ driving conditions, wave perturbations (electric and magnetic field), and electron densities (to identify plasmapause boundary) were collected near the magnetic equatorial plane at a range of distances. These data were compared with Super Dual Auroral Radar Network (SuperDARN) radar (Chisham et al., 2007; Nishitani et al., 2019) line of sight measurements of ionospheric flows to identify the location of wave measurements and for additional contextual information in the ionosphere. As described below, these data provided the lines of evidence needed to identify the wave mode as a PVR. Further details of these radar and satellite measurements can be found in Shi et al. (2017).

The main focus of this study is on the analysis of ground-based E_{GEO}, B_{GEO}, and $\mathbf{Z}$ measurements—the coordinates of ground stations are in Table S1 in the supporting information:

1. Ground-based B_{GEO} from the CARISMA (Mann et al., 2008), THEMIS (Russell et al., 2008), U.S. Geological Survey (USGS) (Love & Finn, 2011), and CANMOS (Nikitina et al., 2016) ground magnetometer networks: These data were examined in Shi et al. (2017), and they will be further used in this study to estimate E_{GEO} using Equation 1. The THEMIS B_{GEO} data are provided in geomagnetic coordinates; for consistency with other data sets, these are rotated to geographic coordinates by using the declination angle from the International Geomagnetic Reference Field model (IGRF-13/year 2014): x points toward geographic North Pole, y points eastward, and z points down to complete the right hand orthogonal set.
2. Ground-based B_{GEO}, E_{GEO}, and $\mathbf{Z}$ from ElectroMagnetic EarthScope (EMScope, the magnetotelluric component of USArray; Schultz, 2010; Schultz et al., 2006–2018, which is in turn a component of the multifaceted EarthScope project; Williams et al., 2010): Each temporary EMScope station, located at a quasi-regular 70-km grid across the contiguous United States, records two horizontal components of E_{GEO} and all three components of B_{GEO} for roughly 3 weeks. This is accomplished using two orthogonal 100-m electric field dipoles (100-m electric cables terminated at each end with electrodes) and a three-axis fluxgate magnetometer. The E_{GEO} and B_{GEO} measurements were provided at 1s cadence and were originally in geomagnetic coordinates; they were rotated to geographic coordinates to be consistent with other measurements. Measurements of E_{GEO}(t) and B_{GEO}(t) are used to calculate the MT impedance tensor (Schultz et al., 2006–2018) as a function of frequency, $\mathbf{Z}(\omega)$. All $\mathbf{Z}$ used in this study are in geographic coordinates. At a location where the MT impedance tensor and magnetic field measurements are available, E_{GEO} can be estimated using Equation 1. The measured and calculated E_{GEO} and B_{GEO} shown in this section were high-pass filtered with a 6.7-mHz cutoff in order to focus on the PVR signal, while the measured E_{GEO} and B_{GEO} shown in section 3 were high-pass filtered with a 1-mHz cutoff to examine a wider-frequency range that includes the Pc5 band.

As shown in Figure 1, the combination of THEMIS satellites, SuperDARN radars, and ground magnetometers enables global specification of wave activity. This event is ideal for studying ULF wave E_{GEO} because of the availability of the above data sets and the fact that Shi et al. (2017) has already characterized the global wave fields (apart from E_{GEO}).

Shi et al. (2017) used observations similar to those shown in Figures 1 and 2 to identify the ULF wave mode as a PVR. We briefly summarize their results:

1. Based on satellite electron density measurements and radar measurements of ionospheric flow speeds, the THEMIS-D satellite is located inside the plasmasphere while THEMIS-E is outside. The dashed line in Figure 1 indicates the plasmapause boundary based on satellite and radar measurements; the darker colors indicate larger flows, consistent with larger flows expected just outside the plasmapause. THEMIS-D has azimuthal ULF electric field (Figure 2b) perturbations that are coherent with ground magnetic perturbations (i.e., have the same frequency and phase relationships over several wave cycles, Figures 2c–2e) observed equatorward of the plasmapause, while THEMIS-E (Figure 2a) observes

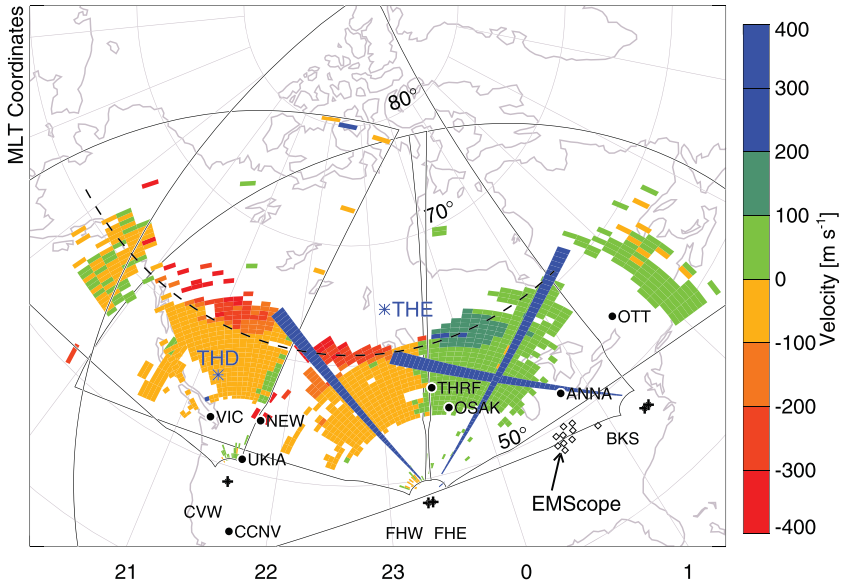

Figure 1. Adapted from Figure 1 in Shi et al. (2017), this figure overlays ground-based observation locations and satellite foot points on ionospheric flow patterns on 25 September 2014 at ~0600 UT. In the figure, blue stars indicate satellite magnetic foot points, black dots indicate ground magnetometer stations, white diamonds indicate EMScope stations, black "+" signs indicate SuparDARN radar sites, blue bars indicate SuperDARN high-resolution beams, color indicates line of sight (LOS) ionosphere velocities in regions with backscatter, and black dashed line indicates latitude corresponding to plasmapause.

irregular electric field variations that are not coherent with the ground magnetometer observations. This suggests a wave mode primarily confined to the plasmasphere.

2. Ground magnetic perturbations have the same frequencies, polarizations, and amplitudes across wide spatial regions (i.e., vary on spatial scales > ~1,000 km, Figures 2c–2e, 2g–2i black lines), consistent with a global mode such as a PVR (Allan et al., 1996). SuperDARN radar observations (Figure 2f) of ionospheric flows are consistent with ground magnetometers; they have the same frequency, and increases/decreases in SuperDARN velocities occur at nearly the same time at different magnetic latitudes. Additional observations in Shi et al. (2017) indicate ground magnetic perturbations have constant frequency across a wide range of longitudes, extending from midnight to the dayside, also consistent with the PVR model.
3. Additional satellite and ground-based polarization analysis from Shi et al. (2017) is consistent with fast mode waves partially trapped in the plasmasphere. Local time variations in polarization are consistent with the location of the wave energy source (substorm related processes including flow bursts and related current systems located near midnight).

In general, a combination of data sets (including satellites and/or radar) is needed to identify PVR and other ULF wave modes (e.g., cavity modes, waveguide modes, and Alfvén modes that do not generate a strong ground magnetic signature). Thus, in order to characterize E_{GEO} related to PVR and other ULF wave modes, coordinated observations such as those shown in Figure 2 are needed.

Figure 3 explores the PVR spatial variation further by showing measured B_{GEO} and measured (sites with IN and KY prefixes) and modeled (all other sites) E_{GEO}; note that agreement between modeled and observed E_{GEO} during this event is excellent (bottom two panels of Figure 3d). Colored circles in this figure are for a frequency-dependent scalar that provides context on local ground conductivity (σ) or the Earth's resistivity ($\rho = 1/\sigma$); in particular, the Berdichevsky average apparent resistivities (Berdichevsky & Dmitriev, 1976) are shown as colored circles for $T_0 = 100$ s perturbations (see Figure S2 for an example of the full, frequency-dependent resistivity at one station). Figure 3b shows the measured B_{GEO} (black) at eight additional ground magnetometers and the modeled E_{GEO} (red) at 0607 UT; E_{GEO} is obtained using Equation 1 and the closest measured EarthScope **Z** (in all cases within 40 km of magnetometer). Both the amplitude and polarization of E_{GEO} vary considerably in response to regional variations in subsurface resistivity. Even for a

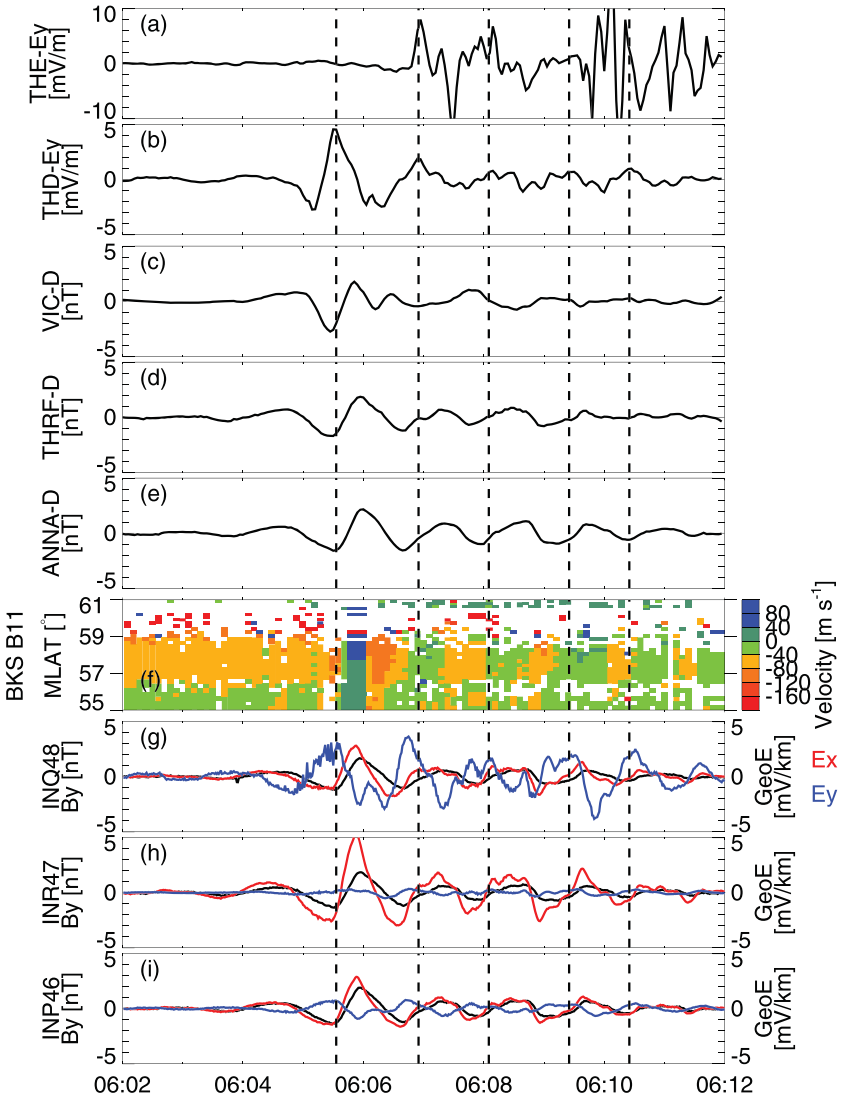

Figure 2. Adapted from results in Shi et al. (2017), this figure shows in situ and ground-based observations during the 25 September 2014 PVR event. From top to bottom, the figure shows THEMIS-E (a) and THEMIS-D (b) satellite east-west electric fields, east-west magnetic perturbation observed by VIC (c), THRF (d), and ANNA (e) ground stations, line of sight velocity in the Blackstone SuperDARN radar beam 11 (f, blue bar originating from BKS in Figure 1), east-west magnetic perturbations (black), and north-south (red)/east-west(blue) electric field perturbations at three EMScope stations (g–i). Dashed lines are shown at times corresponding to the local maxima in the THEMIS-D electric field; these are provided as a reference for the phase relationships with the time series in other panels.

small region with direct measurements of E_{GEO} and B_{GEO} from 10 EMScope stations (Figure 3c), the polarization of E_{GEO} changed significantly while B_{GEO} is constant, for example, comparing INQ48 and INR47 with the rest of the stations. Furthermore, the stations with maximum E_{GEO} do not necessarily have maximum B_{GEO} in Figures 3b and 3c. These points are further demonstrated in the supporting information: Figure S1 shows the time series of B_{GEO} and E_{GEO} for all 10 EMScope stations, Figure S3 shows the measured B_{GEO} and modeled E_{GEO} for the eight magnetometers shown in Figure 3b, and Movie S1 shows the time evolution of Figure 3c from 06:00 to 06:15 UT.

The E_{GEO} and B_{GEO} observations shown here provide further confirmation of the results of Bedrosian and Love (2015): E_{GEO} driven by the magnetospheric ULF wave is nonuniform even in the presence of a spatially uniform B_{GEO}. Thus, ULF waves are subject to the same limitations under the 1-D Earth conductivity assumption as other sources of B_{GEO}. Direct E_{GEO} measurements and/or realistic MT impedances that capture the 3-D conductivity structure of the Earth are needed (Kelbert et al., 2019).

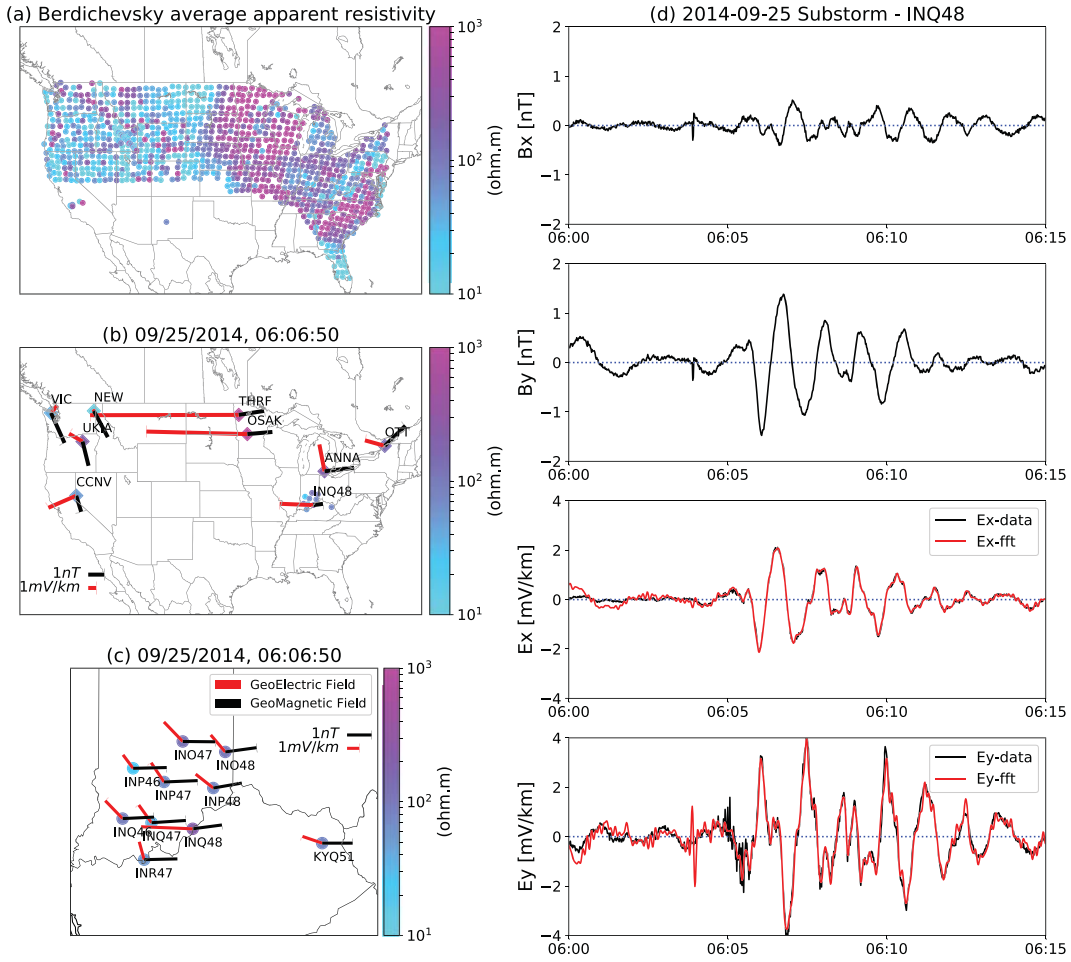

Figure 3. (a) Map showing Berdichevsky average apparent resistivity for $T_0 = 100$ s perturbations. (b) The measured horizontal B_{GEO} (black) and modeled E_{GEO} (red) vectors at 06:06:50 UT on 25 September 2014 from eight ground magnetometer stations shown as black dots in Figure 1 (zoomed out)—E_{GEO} is calculated at the wave period using the measured B_{GEO}, the closest measured EarthScope **Z** (always within 40 km of magnetometer), and Equation 1. (c) The measured horizontal B_{GEO} (black) and measured E_{GEO} (red) vectors at 06:06:50 UT on 25 September 2014 from 10 EMScope stations shown as black diamonds in Figure 1 (zoomed in). (d) Time series of measured horizontal B_{GEO}, measured (black) and modeled (red) E_{GEO} from the INQ48 site.

3. ULF Waves Drive Geoelectric Fields of Significant Amplitude at Midlatitudes

The Shi et al. (2017) PVR event had a frequency of ~10 mHz and occurred during relatively geomagnetically quiet conditions on the nightside at middle to low latitudes, yet PVR and other ULF wave modes can occur in a wider range of conditions, locations, and frequencies. The aim of this section is to demonstrate that ULF waves can drive more extreme E_{GEO} amplitudes at midlatitudes, similar to the latitude range examined in the previous section (~30–60°).

Concerning ULF wave B_{GEO}, Bloom and Singer (1995) examined a similar geographic region to that shown in Figure 1, finding that power for all types of ULF B_{GEO} varies with local time, latitude, frequency, and activity level by roughly 5 orders of magnitude even when restricting to geomagnetic latitudes of 40–55° (see Figure 4 in that study); this corresponds to amplitude variations in B_{GEO} of 2–3 orders of magnitude and suggests that E_{GEO} varies by more than 3 orders of magnitude, given its dependence on both B_{GEO} and **Z** (Equation 1). A few examples of ULF wave activity occurring in similar spatial regions and with similar properties to the PVR shown in this study, but with much larger amplitudes of ~50-100 nT can be found in Fukunishi (1979) (Figure 1 of that study, multiple wave cycles seen in H component by DUR magnetometer 1100–1110 UT) and Villante et al. (2005) (Figure 3b, NUR and HAN magnetometers, multiple wave cycles

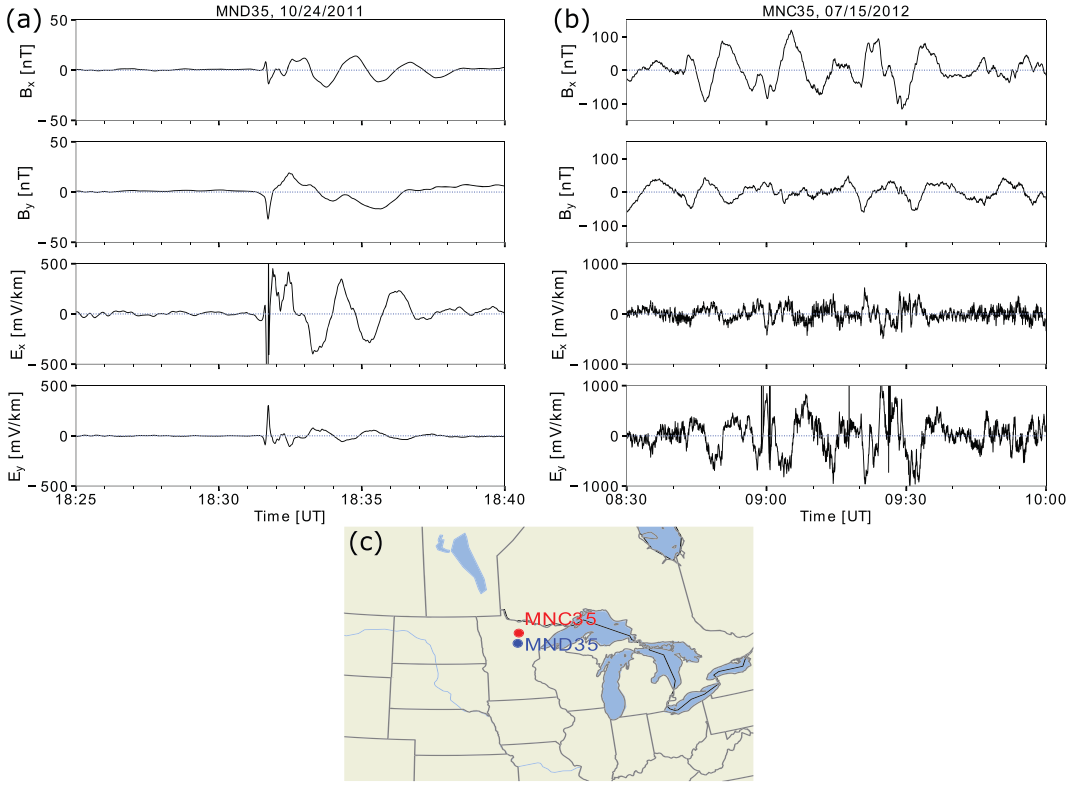

Figure 4. (a) Measurements of B_{GEO} and E_{GEO} from station MND35 during a ULF wave event at the initial stages of the geomagnetic storm on 24 October 2011. From top to bottom, the north-south B_{GEO} component, east-west B_{GEO} component, north-south E_{GEO} component, and east-west E_{GEO} component. (b) The same format as (a) but for station MNC35 and ULF wave activity during the later stages of a geomagnetic storm on 15 July 2012. (c) Map showing the position of stations MND35 and MNC35.

seen in D component from 1105 to 1120 UT). These and numerous other examples of storm time ULF wave activity at midlatitudes (30–60° magnetic latitude) show that ULF wave B_{GEO} amplitudes often reach 100 nT.

No similar case or statistical studies of ULF wave E_{GEO} measurements during storms are available. Thus, we next examine direct measurements of E_{GEO} and B_{GEO} during two storm time ULF wave case studies. The top two panels of Figure 4a show measurements of the north-south and east-west components of B_{GEO} from station MND35 (location shown in Figure 4c) during the initial stages of the geomagnetic storm on 24 October 2011. Multiple wave cycles with roughly 2-min period are seen in the top panel with amplitudes of 10–15 nT. The bottom two panels shown the north-south and east-west components of E_{GEO}, with ULF waves in the north-south component of E_{GEO} having amplitudes of 300–400 mV/km. Figure 4b is the same format as 4a, but for measurements from station MNC35 (location shown in Figure 4c) during the later stages of a geomagnetic storm on 14–15 July 2012. In this event, the Pc5 ULF waves have periods of roughly 5 min, ~100-nT amplitude in B_{GEO} and ~500- to 1,000-mV/km amplitudes in E_{GEO}.

These two ULF wave events occurred during storms with Dst reaching as low as −150 nT (24 October 2011) and −140 nT (14–15 July 2012), yet far more severe storms are possible. There were 40 more intense storms with minimum Dst less than −250 nT in the period January 1957 to May 2005 alone (Gonzalez et al., 2011). Since ULF wave amplitudes increase with increasing geomagnetic activity (e.g., Bloom & Singer, 1995), it is highly likely that more extreme storms will have midlatitude ULF wave E_{GEO} amplitudes that exceed the measured 300–1,000 mV/km E_{GEO} amplitudes shown in Figure 4. At higher latitudes, the amplitudes may be larger since ULF wave amplitudes also generally increase with latitude. It thus seems reasonable that extreme storm time ULF wave E_{GEO} amplitudes at middle and high latitudes could approach the 4- to 10-V/km range, which has been linked to GIC of significant intensity during extreme storms (Winter, 2019). It should also be noted that 1 V/km is at the 1-in-100-year event threshold in 70% of the contiguous United

States (Lucas et al., 2020), although in the specific geographic region shown in Figure 4, the threshold for 1-in-100-year events is much higher (10–20 V/km).

Additional geoelectric hazard analysis focused on ULF wave activity is needed to assess whether different wave modes can drive a significant percentage of 1-in-100-year events, since past hazard analysis did not consider ULF waves:

1. Past analysis (e.g., Lucas et al., 2020) used 1-min cadence B_{GEO} to calculate E_{GEO}, suppressing contributions from most of the ULF range that are above the Nyquist frequency of 8.3 mHz (e.g., waves shown in Figures 2, 3, and the left part of Figure 4).
2. Past analysis did not account for the phenomenology of magnetospheric ULF waves; all sources of B_{GEO} were combined together, whether wave related or not. Thus, the fraction of extreme events that are driven by ULF waves cannot be determined.
3. Past analysis relied on the plane wave assumption to calculate E_{GEO} (section 1), which may not be applicable to all ULF wave events (Murphy & Egbert, 2018).

This study addresses these issues by being the first coordinated investigation linking magnetospheric ULF wave activity to 1 second E_{GEO} measurements and using simultaneous B_{GEO} and E_{GEO} measurements related to ULF waves during storms, but it is not a statistical analysis. Significantly more work is needed to assess the full range of E_{GEO} that might be associated with ULF waves, including a better survey of past storm events for a wider range of wave modes.

4. More Work Is Needed to Characterize ULF Geoelectric Fields

There have been few previous reports linking ULF waves and E_{GEO} (references and discussion in section 1), despite significant past research into the properties of magnetospheric ULF waves and their related B_{GEO} (e.g., Southwood & Hughes, 1983; Takahashi et al., 2006). Moreover, there are very few past measurements of ULF wave E_{GEO}, in contrast to B_{GEO}. We speculate this is due to (1) the lack of widespread, publicly available E_{GEO} and **Z** measurements and (2) the fact that E_{GEO} is not well suited to remote sensing magnetospheric ULF waves due to its dependence on local **Z** (Equation 1).

Though most past ULF wave reviews do not discuss ULF E_{GEO} (e.g., Keiling et al., 2016; McPherron, 2005; Takahashi et al., 2006), a notable exception is the recognition of the relevance of ULF E_{GEO} to magnetotelluric sounding methods (e.g., Gul'el'mi, 1989; Murphy & Egbert, 2018; Orr, 1973; Pilipenko, 1990; Pilipenko & Fedorov, 1994). Pilipenko (1990) noted on page 1207 "One of the most urgent problems in the physics of geomagnetic pulsations is to unify the 'magnetospheric' and 'magnetotelluric' approaches to ULF wave studies." Since the review of Pilipenko (1990), these two research areas have tended to develop in parallel, with little consideration of the impact of one upon the other (cf. Murphy & Egbert, 2018). Three recent developments now provide additional motivation for new studies linking these research areas: (1) the increasingly recognized role of ULF waves in driving GIC (e.g., Belakhovsky et al., 2019), (2) the need for modeled and measured E_{GEO} for tailored assessments of GIC (e.g., Pulkkinen et al., 2017), and (3) increases in the quality, quantity, and availability of E_{GEO} and **Z** measurements from magnetotelluric surveys (e.g., Schultz, 2010).

This letter represents the first coordinated investigation of ULF waves and E_{GEO} using satellite measurements, ground-based radar, ground-based B_{GEO}, and ground-based E_{GEO} measurements; E_{GEO} measurements are supplemented with calculated E_{GEO} using Equation 1 with measured E_{GEO} and **Z**, providing estimates of ULF E_{GEO} across the contiguous United States for a PVR. Additional ULF wave case studies during two storms show ULF wave E_{GEO} amplitudes—whether PVR-related or otherwise—can reach 300–1,000 mV/km. We argue that additional case and statistical studies using similar combinations of data sets and tools are needed to characterize E_{GEO} for other ULF wave modes that may have very different spatial, frequency, and geomagnetic activity dependences than PVR. Significantly more effort is needed to examine the role of magnetospheric ULF waves in the generation of E_{GEO}, including collaboration between the magnetotelluric and magnetospheric ULF wave research communities.

Data Availability Statement

The ground-based magnetic field data used in this work are freely available via the INTERMAGNET (https://www.intermagnet.org, CANMOS and USGS), CARISMA (http://carisma.ca/, CARISMA), and THEMIS

repositories (http://themis.ssl.berkeley.edu/). The code used to produce the modeled electric fields is freely available on github (https://doi.org/10.5281/zenodo.3765861).

Acknowledgments
M. D. H. and X. S. were supported by NASA 80NSSC19K0907. B. S. M. is supported by a U.S. Geological Survey Mendenhall Postdoctoral Fellowship. We acknowledge NASA Contract NAS5-02099 and V. Angelopoulos for use of data from the THEMIS Mission (http://themis.ssl.berkeley.edu/). Specifically, J. W. Bonnell and F. S. Mozer for use of EFI data; S. Mende and C. T. Russell for use of the GMAG data and NSF for support through Grant AGS-1004814. The EarthScope impedance tensors used in this work were retrieved on 8 July 2019, from the Data Management Center of the Incorporated Research Institutions for Seismology SPUD EMTF database (https://doi.org/10.17611/DP/EMTF/USARRAY/TA Kelbert et al., 2011). USArray MT TA project was led by Principal Investigator Adam Schultz and Gary Egbert. USArray TA was funded through NSF Grant EAR0323311, IRIS Subaward 478 and 489 under NSF Cooperative Agreement EAR0350030 and EAR0323309, IRIS Subaward 75MT under NSF Cooperative Agreement EAR0733069 under CFDA 47.050, and IRIS Subaward 05OSUSAGE under NSF Cooperative Agreement EAR1261681 under CFDA 47.050. The facilities of IRIS Data Services, and specifically the IRIS Data Management Center, were used for access to waveforms, related metadata, and/or derived products used in this study (http://service.iris.edu/irisws/timeseries/1/). IRIS Data Services are funded through the Seismological Facilities for the Advancement of Geoscience (SAGE) Award of the National Science Foundation under Cooperative Support Agreement EAR-1851048. The majority of analysis and visualization were completed with the help of free, opensource software tools such as matplotlib (Hunter, 2007), IPython (Pérez & Granger, 2007), and pandas (McKinney, 2010). We thank the World Data Center for Geomagnetism for use of the IGRF-13 calculator (http://wdc.kugi.kyoto-u.ac.jp/igrf/point/index.html).

References

Allan, W., Menk, F. W., Fraser, B. J., Li, Y., & White, S. P. (1996). Are low-latitude Pi2 pulsations cavity/waveguide modes? *Geophysical Research Letters*, *23*(7), 765–768. https://doi.org/10.1029/96GL00661

Angelopoulos, V. (2008). The THEMIS mission. *Space Science Reviews*, *141*(1), 5. https://doi.org/10.1007/s11214-008-9336-1

Bedrosian, P. A., & Love, J. J. (2015). Mapping geoelectric fields during magnetic storms: Synthetic analysis of empirical United States impedances. *Geophysical Research Letters*, *42*, 10,160–10,170. https://doi.org/10.1002/2015GL066636

Belakhovsky, V., Pilipenko, V., Engebretson, M., Sakharov, Y., & Selivanov, V. (2019). Impulsive disturbances of the geomagnetic field as a cause of induced currents of electric power lines. *Journal of Space Weather and Space Climate*, *9*, A18. https://doi.org/10.1051/swsc/2019015

Berdichevsky, M. N., & Dmitriev, V. I. (1976). Distortion of magnetic and electric field by near-surface lateral inhomogeneities. *Acta Geodaetica et Geophysica Hungarica*, *11*, 447–483.

Bloom, R. M., & Singer, H. J. (1995). Diurnal trends in geomagnetic noise power in the Pc 2 through Pc 5 bands at low geomagnetic latitudes. *Journal of Geophysical Research*, *100*(A8), 14,943–14,953. https://doi.org/10.1029/95JA01332

Chisham, G., Lester, M., Milan, S. E., Freeman, M. P., Bristow, W. A., Grocott, A., et al. (2007). A decade of the Super Dual Auroral Radar Network (SuperDARN): Scientific achievements, new techniques and future directions. *Surveys in Geophysics*, *28*(1), 33–109. https://doi.org/10.1007/s10712-007-9017-8

Ferguson, I. J. (2012). Instrumentation and field procedures. In Chave, A. D., & Jones, A. G. E. (Eds.), *The magnetotelluric method: Theory and practice* (pp. 421–479). Cambridge: Cambridge University Press. https://doi.org/10.1017/CBO9781139020138.011

Fukunishi, H. (1979). Latitude dependence of power spectra of magnetic pulsations near L=4 excited by SCC's and SI's. *Journal of Geophysical Research*, *84*(A12), 7191–7200. https://doi.org/10.1029/JA084iA12p07191

Gonzalez, W. D., Echer, E., Clúa de Gonzalez, A. L., Tsurutani, B. T., & Lakhina, G. S. (2011). Extreme geomagnetic storms, recent Gleissberg cycles and space ERA-superintense storms. *Journal of Atmospheric and Solar-Terrestrial Physics*, *73*(11–12), 1447–1453. https://doi.org/10.1016/j.jastp.2010.07.023

Gul'el'mi, A. V. (1989). Reviews of topical problems: Hydromagnetic diagnostics and geoelectric sounding. *Soviet Physics Uspekhi*, *32*(8), 678–696. https://doi.org/10.1070/PU1989v032n08ABEH002747

Hunter, J. D. (2007). Matplotlib: A 2D graphics environment. *Computing in Science & Engineering*, *9*(3), 90–95. https://doi.org/10.1109/MCSE.2007.55

Jacobs, J. A., Kato, Y., Matsushita, S., & Troitskaya, V. A. (1964). Classification of geomagnetic micropulsations. *Journal of Geophysical Research*, *69*(1), 180–181. https://doi.org/10.1029/JZ069i001p00180

Keiling, A., Lee, D.-H., & Nakariakov, V. (2016). *Low-frequency waves in space plasmas* (Vol. 216). John Wiley & Sons. https://agupubs.onlinelibrary.wiley.com/doi/book/10.1002/9781119055006

Kelbert, A., Balch, C. C., Pulkkinen, A., Egbert, G. D., Love, J. J., Rigler, E. J., & Fujii, I. (2017). Methodology for time-domain estimation of storm time geoelectric fields using the 3-D magnetotelluric response tensors. *Space Weather*, *15*, 874–894. https://doi.org/10.1002/2017SW001594

Kelbert, A., Bedrosian, P. A., & Murphy, B. S. (2019). The first 3D conductivity model of the contiguous United States. In *Geomagnetically Induced Currents from the Sun to the Power Grid* (pp. 127–151). American Geophysical Union (AGU). https://doi.org/10.1002/9781119434412.ch8

Kelbert, A., Egbert, G. D., & Schultz, A. (2011). IRIS DMC data services products: EMTF. The magnetotelluric transfer functions. *National Geoelectromagnetic Facility Technical Report*. https://doi.org/10.17611/DP/EMTF.1

Lee, D.-H., & Kim, K. (1999). Compressional MHD waves in the magnetosphere: A new approach. *Journal of Geophysical Research*, *104*(A6), 12,379–12,385. https://doi.org/10.1029/1999JA900053

Lee, D.-H., & Takahashi, K. (2006). MHD eigenmodes in the inner magnetosphere. In *Magnetospheric ULF waves: Synthesis and new directions* (Vol. 169, pp. 73). https://doi.org/10.1029/169GM07

Love, J. J., & Finn, C. A. (2011). The USGS geomagnetism program and its role in space weather monitoring. *Space Weather*, *9*, 07001. https://doi.org/10.1029/2011SW000684

Love, J. J., Lucas, G. M., Bedrosian, P. A., & Kelbert, A. (2019). Extreme-value geoelectric amplitude and polarization across the northeast United States. *Space Weather*, *17*, 379–395. https://doi.org/10.1029/2018SW002068

Lucas, G. M., Love, J. J., & Kelbert, A. (2018). Calculation of voltages in electric power transmission lines during historic geomagnetic storms: An investigation using realistic Earth impedances. *Space Weather*, *16*, 185–195. https://doi.org/10.1002/2017SW001779

Lucas, G. M., Love, J. J., Kelbert, A., Bedrosian, P. A., & Rigler, E. J. (2020). A 100-year geoelectric hazard analysis for the U.S. high-voltage power grid. *Space Weather*, *18*, e2019SW002329. https://doi.org/10.1029/2019SW002329

Mann, I. R., Milling, D. K., Rae, I. J., Ozeke, L. G., Kale, A., Kale, Z. C., et al. (2008). The upgraded CARISMA magnetometer array in the THEMIS Era. *Space Science Reviews*, *141*(1), 413–451. https://doi.org/10.1007/s11214-008-9457-6

McKinney, W. (2010). Data structures for statistical computing in python. In *Proceedings of the 9th Python in Science Conference*, *445*, Austin, TX, (pp. 51–56).

McPherron, R. L. (2005). Magnetic pulsations: Their sources and relation to solar wind and geomagnetic activity. *Surveys in Geophysics*, *26*(5), 545–592. https://doi.org/10.1007/s10712-005-1758-7

Murphy, B. S., & Egbert, G. D. (2018). Source biases in midlatitude magnetotelluric transfer functions due to Pc3-4 geomagnetic pulsations. *Earth, Planets and Space*, *70*(1), 12. https://doi.org/10.1186/s40623-018-0781-0

Nikitina, L., Trichtchenko, L., & Boteler, D. H. (2016). Assessment of extreme values in geomagnetic and geoelectric field variations for Canada. *Space Weather*, *14*, 481–494. https://doi.org/10.1002/2016SW001386

Nishitani, N., Ruohoniemi, J. M., Lester, M., Baker, J., Koustov, A. V., Shepherd, S., et al. (2019). Review of the Accomplishments of Mid-latitude Super Dual Auroral Radar Network (SuperDARN) HF radars. *Progress in Earth and Planetary Science*, *6*, 27. https://doi.org/10.1186/s40645-019-0270-5

North American Electric Reliability Corporation (NERC) (2012). Special reliability assessment interim report: Effects of geomagnetic disturbances on the bulk power system.

Orr, D. (1973). Magnetic pulsations within the magnetosphere: A review. *Journal of Atmospheric and Terrestrial Physics*, *35*, 1–50. https://doi.org/10.1016/0021-9169(73)90214-6

Pérez, F., & Granger, B. E. (2007). IPython: A system for interactive scientific computing. *Computing in Science & Engineering*, *9*(3), 21–29. https://doi.org/10.1109/MCSE.2007.53

Pilipenko, V. A. (1990). ULF waves on the ground and in space. *Journal of Atmospheric and Terrestrial Physics*, *52*, 1193–1209. https://doi.org/10.1016/0021-9169(90)90087-4

Pilipenko, V. A., & Fedorov, E. N. (1994). Magnetotelluric sounding of the crust and hydrodynamic monitoring of the magnetosphere with the use of ULF waves. *Washington DC American Geophysical Union Geophysical Monograph Series*, *81*, 283–292. https://doi.org/10.1029/GM081p0283

Pulkkinen, A., Bernabeu, E., Thomson, A., Viljanen, A., Pirjola, R., Boteler, D., et al. (2017). Geomagnetically induced currents: Science, engineering, and applications readiness. *Space Weather*, *15*, 828–856. https://doi.org/10.1002/2016SW001501

Pulkkinen, A., & Kataoka, R. (2006). S-transform view of geomagnetically induced currents during geomagnetic superstorms. *Geophysical Research Letters*, *33*, L12108. https://doi.org/10.1029/2006GL025822

Russell, C. T., Chi, P. J., Dearborn, D. J., Ge, Y. S., Kuo-Tiong, B., Means, J. D., et al. (2008). THEMIS ground-based magnetometers. *Space Science Reviews*, *141*(1), 389–412. https://doi.org/10.1007/s11214-008-9337-0

Schultz, A. (2010). EMScope: A continental scale magnetotelluric observatory and data discovery resource. *Data Science Journal*, *8*, IGY6–IGY20. https://doi.org/10.2481/dsj.ss_igy-009

Schultz, A., Egbert, G. D., Kelbert, A., Peery, T., Clote, V., Fry, B., et al. (2006–2018). USArray TA magnetotelluric transfer functions. https://doi.org/10.17611/DP/EMTF/USARRAY/TA

Shi, X., Baker, J. B. H., Ruohoniemi, J. M., Hartinger, M. D., Frissell, N. A., & Liu, J. (2017). Simultaneous space and ground-based observations of a plasmaspheric virtual resonance. *Journal of Geophysical Research: Space Physics*, *122*, 4190–4209. https://doi.org/10.1002/2016JA023583

Southwood, D. J., & Hughes, W. J. (1983). Theory of hydromagnetic-waves in the magnetosphere. *Space Science Reviews*, *35*(4), 301–366. https://doi.org/10.1007/BF00169231

Takahashi, K., Berube, D., Lee, D.-H., Goldstein, J., Singer, H. J., Honary, F., & Moldwin, M. B. (2009). Possible evidence of virtual resonance in the dayside magnetosphere. *Journal of Geophysical Research*, *114*, A05206. https://doi.org/10.1029/2008JA013898

Takahashi, K., Chi, P. J., Denton, R. E., & Lysak, R. L. (2006). *Magnetospheric ULF waves: Synthesis and new directions* (Vol. 169). Wiley Blackwell. https://doi.org/10.1029/GM169

Thomson, A. W. P. (2007). Geomagnetic hazards. In D. Gubbins, & E. Herrero-Bervera (Eds.), *Encyclopedia of geomagnetism and paleomagnetism* (pp. 316–319). Dordrecht: Springer Netherlands. https://doi.org/10.1007/978-1-4020-4423-6_117

Villante, U., Piersanti, M., di Giuseppe, P., Vellante, M., Zhang, T. L., & Magnes, W. (2005). Sudden commencement event of 17 April 2002: Aspects of the geomagnetic response at low latitudes. *Journal of Geophysical Research*, *110*, A12S23. https://doi.org/10.1029/2004JA010978

Williams, M. L., Fischer, K. M., Freymueller, J. T., Tikoff, B., Tréhu, A. M., & others (2010). *Unlocking the secrets of the North American continent: An EarthScope science plan for 2010–2020*. EarthScope.

Winter, L. M. (2019). Geomagnetically induced currents from extreme space weather events. In *Geomagnetically induced currents from the Sun to the power grid* (pp. 195–203). American Geophysical Union (AGU). https://doi.org/10.1002/9781119434412.ch11